JOURNAL OF GEOPHYSICAL RESEARCH, VOL. 95, NO. B7, PAGES 11,301–11,315, JULY 10, 1990

Vertical Seismic Profile Synthetics by Dynamic Ray Tracing in Laterally Varying Layered Anisotropic Structures

DIRK GAJEWSKI[1]

Department of Geophysics, Stanford University, Stanford, California

IVAN PŠENČÍK[2]

Geophysical Institute, Czechoslovak Academy of Sciences, Prague, Czechoslovakia

Dynamic ray tracing (DRT) is important in evaluating high-frequency seismic wave fields in complicated structures. Two formulations of the DRT equations for inhomogeneous anisotropic media are presented. One of them is represented by the classical DRT system, suggested by Červený 15 years ago. Both systems are specified in Cartesian coordinates. The DRT equations are supplemented with formulae for the transformation of DRT across a smoothly curved interface between two inhomogeneous anisotropic media. Červený's formulation of the DRT is applied to the computation of vertical seismic profile (VSP) synthetics. The results of DRT are used for the evaluation of the geometrical spreading and of the coefficients of the paraxial ray approximation for travel times and ray amplitudes. In addition, the DRT is also used in the interval ray tracing procedure, a procedure searching for rays starting from the source and terminating in a specified interval on a profile. Results of numerical modeling of VSP measurements in a three-dimensional laterally varying structure consisting of isotropic and anisotropic layers separated by curved interfaces are presented. Ray diagrams of selected elementary waves, time-distance curves, and multisource three-component VSP synthetics generated for two different source locations calculated for the anisotropic model are compared with the results determined for a reference isotropic model. The latter is obtained by averaging phase velocities of the anisotropic model. This comparison clearly shows the effects of anisotropy and the lateral variation of the model on seismic wave fields. The reliability of the ray synthetics is briefly discussed.

INTRODUCTION

The evaluation of ray amplitudes, as well as the paraxial ray approximation of travel times and ray amplitudes, requires the knowledge of the partial derivatives of coordinates of a ray and of the components of the slowness vectors along this ray with respect to ray parameters. These quantities can be determined approximately by substituting the partial derivatives by finite differences and evaluating the differences from the values on nearby rays. This approach was adopted by *Gajewski and Pšenčík* [1987, 1988] and *Shearer* [1988]. It is simple and does not require knowledge of the transformation laws for the partial derivatives across interfaces. It may, however, yield inaccurate results in some situations.

Another procedure to evaluate the partial derivatives is based on a solution of a system of linear differential equations, the dynamic ray tracing (DRT) equations. This procedure is widely used in ray computations for isotropic media. The DRT equations can be written in different coordinate systems. For example, *Červený et al.* [1974] wrote the DRT system in Cartesian coordinates. Mostly, however, the DRT equations for isotropic media are written in the so-called ray-centered coordinate system in which the number of equations to be solved is considerably reduced.

Dynamic ray tracing equations for smoothly inhomogeneous anisotropic media were proposed by *Červený* [1972]. They were derived in Cartesian coordinates. *Nomofilov* [1981] derived a general DRT system which could also be applied to inhomogeneous anisotropic media. It was written in a coordinate system which resembled the ray-centered coordinates for isotropic media. A similar approach was used by *Hanyga* [1982]. *Norris* [1987] derived formulae for a transformation of the DRT across curved interfaces separating homogeneous anisotropic layers. Inside the layers, he used the "Cartesian" DRT equations of *Červený* [1972], specified for homogeneous anisotropic media. Norris performed the transformation of DRT across an interface in a special local orthogonal coordinate system so that at each interface a transformation from general Cartesian coordinates into the special coordinate system and back was required. A similar procedure was used by *Virieux et al.* [1988] for layered isotropic media. *Norris* [1987] presented numerical examples of the application of the DRT to compute pulses propagating in anisotropic fiber-reinforced composites. Seismological applications of the "Cartesian" dynamic ray tracing on *qP* waves in smooth media without interfaces are given by *Kendall and Thomson* [1989]. Besides the numerical results these authors also present several possible forms of DRT equations.

Here we concentrate on the "Cartesian" DRT, mostly on the classical system derived by *Červený* [1972]. In addition, an alternative DRT system is also given which can be useful in special situations. Then we derive formulae for the transformation of the DRT system across a smooth interface between two generally varying anisotropic media. The transformation formulae are derived in the way used by *Červený et al.* [1974] for a similar problem in isotropic media. In contrast to work by *Norris* [1987] and *Virieux et al.* [1988], the procedure presented here requires no transformation of coordinates at the

[1]Now at Institute of Geophysics, Technical University of Clausthal, Clausthal-Zellerfeld, Federal Republic of Germany.

[2]Visiting Scientist at the Earth Science Division, Lawrence Berkeley Laboratory, Berkeley, California.

Paper number 89JB01539.
0148-0227/90/89JB-01539$05.00

interface. Numerical examples of the application of DRT to compute vertical seismic profile (VSP) synthetics for a three–dimensional (3–D) anisotropic layered model show possibilities of the ray code. In order to separate the effects of anisotropy from the effects of structural variations, the above results are compared with the calculations obtained for a reference isotropic model. The reference model is determined by averaging phase velocities of the anisotropic model. Finally, the reliability of the presented results is briefly discussed.

The component notation for vectors and matrices is used throughout the paper. The Einstein convention applies over repeated right-hand suffixes. The lowercase indices take values 1, 2, and 3, the capital indices take values 1 and 2.

BASIC FORMULAE FOR ANISOTROPIC MEDIA

In the following, we summarize the most important formulae of the ray method for inhomogeneous anisotropic media. More details are given by *Červený* [1972] or, e.g., *Gajewski and Pšenčík* [1987].

We seek a solution to the equation of motion for inhomogeneous, perfectly elastic anisotropic media in the form

$$u_i(x_j,t)=U_i(x_j)\exp[-i\omega(t-\tau(x_j))] \tag{1}$$

The amplitude vector $U_i(x_j)$ and the phase function $\tau(x_j)$ can be determined from the basic system of equations of the ray method for inhomogeneous anisotropic media,

$$(\Gamma_{jk}-\delta_{jk})U_k=0 \tag{2}$$

$$a_{ijkl}p_iU_{k,j}+\rho^{-1}(\rho a_{ijkl}p_lU_k)_{,j}=0 \tag{3}$$

In (2), we denote

$$\Gamma_{jk}=a_{ijkl}p_ip_l \qquad p_i=\frac{\partial\tau}{\partial x_i} \qquad a_{ijkl}=\frac{c_{ijkl}}{\rho} \tag{4}$$

where $c_{ijkl}=c_{ijkl}(x_m)$ is a tensor of elastic parameters and ρ is the density.

The phase function $\tau(x_j)$ can be found by solving the ray tracing equations

$$\begin{aligned}\frac{dx_i}{d\tau}&=\frac{1}{2}\frac{\partial G}{\partial p_i}=a_{ijkl}p_lg_jg_k\\ \frac{dp_i}{d\tau}&=-\frac{1}{2}\frac{\partial G}{\partial x_i}=-\frac{1}{2}a_{mjkl,i}p_mp_lg_jg_k\end{aligned} \tag{5}$$

In (5), $G=G(x_i,p_i)$ denotes one of the three eigenvalues of the matrix Γ_{jk}, which corresponds to the considered wave. Symbol g_i indicates the corresponding eigenvector. The eigenvalue G satisfies the equation

$$G=a_{ijkl}p_ip_lg_jg_k=1 \tag{6}$$

which is sometimes called the eikonal equation. Solutions of the ray-tracing system (5), including its initial values, must satisfy the eikonal equation for any time τ.

The amplitude $U_i(\bar{x}_j)$ at the point $\bar{x}_j$ of a ray Ω specified by the ray parameters γ_1, γ_2 (e.g., takeoff angles at the source) can be found by solving equation (3) along Ω. It is given by

$$U_i(\bar{x}_j)=\Psi(\gamma_1,\gamma_2)[\rho(\bar{x}_j)\det X_{mn}(\bar{x}_j)]^{-1/2}g_i(\bar{x}_j) \tag{7}$$

In (7), $\Psi=\Psi(\gamma_1,\gamma_2)$ is a function constant along the ray Ω, and it describes the properties of the source. The symbol X_{mn} denotes the partial derivative

$$X_{mn}=\frac{\partial x_m}{\partial\gamma_n} \tag{8}$$

where γ_1, γ_2 are the above mentioned ray parameters and $\gamma_3=\tau$.

The matrix X_{mn} plays also an important role in the paraxial ray approximation of the travel time and slowness vector in a vicinity of the ray Ω (knowledge of the slowness vector in a vicinity of Ω is important for the determination of ray amplitudes in this vicinity); see *Gajewski and Pšenčík* [1987],

$$\tau(x_j)=\tau(\bar{x}_j)+p_k(\bar{x}_j)(x_k-\bar{x}_k)+\frac{1}{2}N_{ik}(\bar{x}_j)(x_i-\bar{x}_i)(x_k-\bar{x}_k) \tag{9}$$

$$p_i(x_j)=p_i(\bar{x}_j)+N_{ik}(\bar{x}_j)(x_k-\bar{x}_k) \tag{10}$$

In (9) and (10), $\bar{x}_j$ denotes again a point on the ray Ω and N_{ik} is a matrix of the second Cartesian partial derivatives of the travel time field. It is given by

$$N_{ik}=\frac{\partial^2\tau}{\partial x_i\partial x_k}=\frac{\partial p_i}{\partial x_k}=Y_{ij}(\mathbf{X}^{-1})_{jk} \tag{11}$$

where

$$Y_{mn}=\frac{\partial p_m}{\partial\gamma_n} \tag{12}$$

The elements $X_{i3}=\partial x_i/\partial\tau$ and $Y_{i3}=\partial p_i/\partial\tau$ of the matrices X_{mn} and Y_{mn} can be determined directly from the ray-tracing equations (5). Thus it remains to determine those elements which represent derivatives with respect to γ_1 and γ_2. One possibility of evaluating X_{ij} and Y_{ij} was suggested and used by *Gajewski and Pšenčík* [1987] and *Shearer* [1988]. In it, partial derivatives were substituted by finite differences and evaluated from the values on nearby rays. Another possibility is the evaluation of X_{ij} and Y_{ij} by solving numerically the DRT equations.

DYNAMIC RAY TRACING

Dynamic Ray Tracing in a Smooth Inhomogeneous Anisotropic Medium

The DRT equations are obtained by differentiating the ray–tracing equations (5) with respect to the ray parameters γ_J

$$\begin{aligned}\frac{dX_{iJ}}{d\tau}&=\frac{1}{2}\left[\frac{\partial^2G}{\partial p_i\partial x_k}X_{kJ}+\frac{\partial^2G}{\partial p_i\partial p_k}Y_{kJ}\right]\\ \frac{dY_{iJ}}{d\tau}&=-\frac{1}{2}\left[\frac{\partial^2G}{\partial x_i\partial x_k}X_{kJ}+\frac{\partial^2G}{\partial x_i\partial p_k}Y_{kJ}\right]\end{aligned} \tag{13}$$

As we can see, to make the system of linear differential equations useful for a numerical evaluation of X_{ij} and Y_{ij}, it is necessary to find expressions for the second partial derivatives of the eigenvalue G. This can be done in several ways.

Červený [1972] obtained the second derivatives of G by differentiating the expressions for its first derivatives,

$$\frac{\partial G}{\partial z_i}=\frac{\partial\Gamma_{jk}}{\partial z_i}\frac{D_{jk}}{D_{II}} \tag{14}$$

where z_i may be either x_i or p_i. In (14), D_{ij} is given by

$$D_{ij}=\frac{1}{2}\varepsilon_{ikl}\varepsilon_{jmn}(\Gamma_{km}-G\,\delta_{km})(\Gamma_{ln}-G\,\delta_{ln}) \tag{15}$$

where ε_{ikl} is the third-order alternating tensor (Levi-Civita's tensor). By comparison with (5), it can be shown that

$$\frac{D_{ij}}{D_{II}}=g_ig_j \tag{16}$$

Differentiating (14) with respect to z_s, we get

$$\frac{\partial^2 G}{\partial z_i \partial z_s}=\frac{\partial^2 \Gamma_{jk}}{\partial z_i \partial z_s}\frac{D_{jk}}{D_{mn}}+\frac{\partial \Gamma_{jk}}{\partial z_i}\frac{\partial}{\partial z_s}\left[\frac{D_{jk}}{D_{mn}}\right] \tag{17}$$

The expression for a derivative of D_{ij} with respect to z_s is obtained by direct differentiation of (15), which yields

$$\frac{\partial D_{ij}}{\partial z_s}=\frac{1}{\beta}\left[\varepsilon_{ikl}\varepsilon_{jmn}\frac{\partial \Gamma_{km}}{\partial z_s}\Gamma_{ln}-\frac{\partial \Gamma_{kk}}{\partial z_s}\delta_{ij}+\frac{\partial \Gamma_{ij}}{\partial z_s}\right]+\frac{\partial D_{ij}}{\partial G}\frac{\partial G}{\partial z_s} \tag{18}$$

Due to the equation

$$\frac{\partial G}{\partial x_k}X_{kl}+\frac{\partial G}{\partial p_k}Y_{kl}=0 \tag{19}$$

which follows from the differentiation of the eikonal equation (6) with respect to γ_J, the last term on the right-hand side of (18) does not contribute to the right-hand side of the DRT equations (13); see detailed discussion by *Kendall and Thomson* [1989]. Solutions of the DRT equations, including their initial values, must satisfy (19) at any time τ.

An alternative method of determining the second derivatives of the eigenvalue G of the matrix Γ_{jk} is based on knowledge of all three eigenvalues and eigenvectors of Γ_{jk} at any point of a considered ray. This procedure can be useful in situations where the eigenvalues and eigenvectors of the matrix Γ_{jk} are easy to determine (e.g., for higher symmetries of the anisotropy like hexagonal). To distinguish between individual eigenvectors and eigenvalues, we mark them by right-hand superscripts in brackets.

It is shown in the appendix that the second derivative of the eigenvalue $G^{(m)}$ with respect to z_r, where z_r may be either x_r or p_r, can be written as

$$\frac{\partial^2 G^{(m)}}{\partial z_r \partial z_s}=\frac{\partial^2 \Gamma_{jk}}{\partial z_r \partial z_s}g_j^{(m)}g_k^{(m)}+2\sum_{n=1}^{3}{}^{(n\neq m)}(G^{(m)}-G^{(n)})^{-1}A_r^{(mn)}A_s^{(mn)} \tag{20}$$

where

$$A_r^{(mn)}=\frac{\partial \Gamma_{jk}}{\partial z_r}g_j^{(m)}g_k^{(n)} \tag{21}$$

and $\sum^{(n\neq m)}_{n}$ denotes the summation in which the term for $n=m$ is not included.

The right-hand side of (20) is singular wherever $G^{(m)}=G^{(n)}$ for $n\neq m$. This condition is equivalent to $V_m=V_n$ for $n\neq m$, see the appendix, where V_m and V_n are the phase velocities of the waves corresponding to the mth and nth eigenvalue. Relation (20) is universal for quasi-compressional waves (since we do not expect the phase velocity of quasi-compressional waves to be equal to the phase velocity of the quasi-shear waves). Relation (20) is singular in regions or directions in which the phase velocities of the two quasi-shear waves are the same, i.e., where the wave surfaces of the two quasi-shear waves touch or intersect each other. In an isotropic medium, relation (20) is singular everywhere.

Let us note that the same singularity exists in relation (17) since D_{mm} is zero wherever $G^{(m)}=G^{(n)}$ for $m\neq n$. This follows from the following considerations. For D_{mm}, equation (15) yields

$$D_{mm}=\frac{1}{\beta^2}(\Gamma_{kk}\Gamma_{ij}-\Gamma_{jk}\Gamma_{jk}-4\Gamma_{jj}G+6G^2)$$

This can be written in the matrix notation

$$\mathrm{tr}\mathbf{D}=\frac{1}{\beta^2}(\det\boldsymbol{\Gamma}\,\mathrm{tr}\boldsymbol{\Gamma}^{-1}-2G\,\mathrm{tr}\boldsymbol{\Gamma}+3G^2)$$

where tr and det indicate the trace and the determinant, respectively, of the corresponding matrix. The right-hand side of the above equation can be expressed in terms of the eigenvalues $G^{(m)}$ of the matrix Γ_{jk} through the relations $\det\boldsymbol{\Gamma}=G^{(1)}G^{(2)}G^{(3)}$, $\mathrm{tr}\boldsymbol{\Gamma}=(G^{(1)}+G^{(2)}+G^{(3)})$ and $\mathrm{tr}\boldsymbol{\Gamma}^{-1}=[(G^{(1)})^{-1}+(G^{(2)})^{-1}+(G^{(3)})^{-1}]$. In this way,

$$\mathrm{tr}\mathbf{D}=\frac{1}{\beta^2}(G^{(2)}G^{(3)}+G^{(1)}G^{(3)}+G^{(1)}G^{(2)}-2(G^{(1)}+G^{(2)}+G^{(3)})G+3G^2)$$

For the eigenvalue $G=G^{(m)}=G^{(n)}$ for $n\neq m$, this equation yields $D_{mm}=0$.

Prior to the application of the above DRT systems to inhomogeneous layered anisotropic media, two steps must be performed. In the first, initial values for the DRT system must be specified at the source. In the other step, the laws governing the transformation of DRT across interfaces between anisotropic layers have to be determined. Since we consider point sources situated in an isotropic layer, we can refer for the former step to any paper dealing with DRT in isotropic media [see, e.g., *Červený et al.*, 1974; *Virieux et al.*, 1988]. The second step is considered in the next section.

Transformation of Dynamic Ray Tracing Across an Interface

Let us consider an interface specified by

$$f(x_j)=0 \tag{22}$$

The function $f(x_j)$ is supposed to have continuous partial derivatives up to the second order in a vicinity of the point of incidence of a ray at the interface. The unit normal to the interface at the point of incidence is

$$n_i=\pm\frac{\partial f}{\partial x_i}\left[\frac{\partial f}{\partial x_k}\frac{\partial f}{\partial x_k}\right]^{-1/2} \tag{23}$$

In (23), we choose the sign so that the normal points into the medium in which the incident wave propagates.

The initial values for the ray-tracing system (5) along a ray of a generated wave, i.e., a reflected or transmitted wave, can be written in the following form:

$$\hat{x}_i(\gamma_K,T(\gamma_J))=x_i(\gamma_K,T(\gamma_J)) \tag{24}$$

$$\hat{p}_i(\gamma_K,T(\gamma_J))=p_i(\gamma_K,T(\gamma_J))+n_i[\xi-n_ip_i(\gamma_K,T(\gamma_J))] \tag{25}$$

Here symbols with carets denote the quantities corresponding to the generated wave. As before, γ_K, $K=1,2$, denote ray parameters. T indicates the time at which the considered ray, specified by γ_K, hits the interface. Thus

$$T=T(\gamma_K) \tag{26}$$

is another form of the equation of interface (22). Equation (25) simply follows from the formula derived by *Fedorov* [1968], see equation (17) of *Gajewski and Pšenčík* [1987],

$$p_i=b_i+\xi n_i \tag{27}$$

which holds for the slowness vector of any wave at the point of incidence. Vector b_i is the vectorial component of the slowness vector in the plane tangential to the interface at the point of incidence. From the equality of travel times of the incident and any generated waves along the interface it follows that the vector b_i is the same for all waves at the point of incidence. The quantity ξ is a projection of the slowness vector on the normal to the interface, which can differ for different waves. Methods to determine ξ are described by *Fedorov* [1968]; for a brief discussion, see also *Gajewski and Pšenčík* [1987].

The sought relations between $\hat{X}_{iM}, \hat{Y}_{iM}$ and X_{iM}, Y_{iM} are obtained by differentiating (24) and (25) with respect to γ_M. Let us use z_i to denote either x_i or p_i and Z_{iM} ($\hat{Z}_{iM}$) to denote quantities X_{iM} ($\hat{X}_{iM}$) or Y_{iM} ($\hat{Y}_{iM}$). The terms $\partial z_i(\gamma_K, T(\gamma_J))/\partial\gamma_M$ which result from the differentiation of (24) and (25) are partial derivatives along the interface. They are connected with Z_{iM} (which are partial derivatives along the wave front) in the following way,

$$\frac{\partial z_i(\gamma_K, T(\gamma_J))}{\partial\gamma_M} = \left.\frac{\partial z_i}{\partial\gamma_M}\right|_{\tau=T} + \frac{\partial z_i}{\partial\tau}\frac{\partial T}{\partial\gamma_M} = Z_{iM} + Z_{i3}T_M \tag{28}$$

Likewise, for $\partial\hat{z}_i(\gamma_K, T(\gamma_J))/\partial\gamma_M$, we can write

$$\frac{\partial\hat{z}_i(\gamma_K, T(\gamma_J))}{\partial\gamma_M} = \hat{Z}_{iM} + \hat{Z}_{i3}T_M \tag{29}$$

The quantities Z_{i3} ($\hat{Z}_{i3}$) denote either $\partial x_i/\partial\tau$ ($\partial\hat{x}_i/\partial\tau$) or $\partial p_i/\partial\tau$ ($\partial\hat{p}_i/\partial\tau$), i.e., the quantities which can be directly determined from the ray tracing equations. The quantity $T_M = \partial T/\partial\gamma_M$ can be determined from (22) in which we insert $x_i = x_i(\gamma_K, T(\gamma_J))$ and differentiate with respect to γ_M. Taking into account (23), we get

$$n_j(X_{jM} + X_{j3}T_M) = 0$$

from which

$$T_M = -\frac{n_j X_{jM}}{n_k X_{k3}} \tag{30}$$

Now, if we differentiate (24) and (25) with respect to γ_M and consider (28) and (29), we arrive at

$$\hat{X}_{iM} = X_{iM} + (X_{i3} - \hat{X}_{i3})T_M \tag{31}$$

$$\hat{Y}_{iM} = Y_{iM} + (Y_{i3} - \hat{Y}_{i3})T_M + \frac{\partial n_i}{\partial\gamma_M}(\xi - n_l p_l) + n_i\left[\frac{\partial\xi}{\partial\gamma_M} - \frac{\partial n_l}{\partial\gamma_M}p_l - n_l Y_{lM} - (n_l Y_{l3})T_M\right] \tag{32}$$

In (32), we must specify the partial derivatives $\partial n_l/\partial\gamma_M$ and $\partial\xi/\partial\gamma_M$. The determination of $\partial n_l/\partial\gamma_M$ is straightforward,

$$\frac{\partial n_l}{\partial\gamma_M} = \frac{\partial n_l}{\partial x_k}(X_{kM} + X_{k3}T_M) \tag{33}$$

The expression for $\partial\xi/\partial\gamma_M$ can be obtained by the differentiation of the eikonal equation

$$G(\hat{x}_i, \hat{p}_i) = 1 \tag{34}$$

corresponding to the generated wave at the point of incidence, with respect to γ_M. We get

$$\frac{\partial G}{\partial\hat{x}_k}(\hat{X}_{kM} + \hat{X}_{k3}T_M) + \frac{\partial G}{\partial\hat{p}_k}(\hat{Y}_{kM} + \hat{Y}_{k3}T_M) = 0 \tag{35}$$

analogous to (19). If we insert relations (31) and (32) into (35) and substitute $\partial G/\partial\hat{x}_k$, $\partial G/\partial\hat{p}_k$ by $-\hat{Y}_{k3}$, $\hat{X}_{k3}$ (see (5)), we can solve (35) for $\partial\xi/\partial\gamma_M$. We get

$$\frac{\partial\xi}{\partial\gamma_M} = (\hat{X}_{k3}n_k)^{-1}\left\{\hat{Y}_{i3}(X_{iM} + X_{i3}T_M) - \hat{X}_{i3}\left[(Y_{iM} + Y_{i3}T_M) + \frac{\partial n_i}{\partial\gamma_M}(\xi - n_l p_l) - n_i\left[\frac{\partial n_l}{\partial\gamma_M}p_l + n_l Y_{lM} + n_l Y_{l3}T_M\right]\right]\right\} \tag{36}$$

Inserting this into (32), after some arrangements we get the final form of transformation equations

$$\hat{X}_{iM} = X_{iM} + (X_{i3} - \hat{X}_{i3})T_M \tag{37a}$$

$$\hat{Y}_{iM} = Y_{iM} + (Y_{i3} - \hat{Y}_{i3})T_M + (\xi - n_l p_l)\left[\frac{\partial n_i}{\partial\gamma_M} - n_i(\hat{X}_{j3}n_j)^{-1}\hat{X}_{k3}\frac{\partial n_k}{\partial\gamma_M}\right] - n_i\left\{(\hat{X}_{j3}n_j)^{-1}\left[\hat{X}_{k3}(Y_{kM} + Y_{k3}T_M) - \hat{Y}_{k3}(X_{kM} + X_{k3}T_M)\right]\right\} \tag{37b}$$

where T_M and $\partial n_k/\partial\gamma_M$ are given by (30) and (33).

We can see from (37) that the initial conditions for dynamic ray tracing along a ray of a generated wave depend on several factors at the point of incidence. Through the quantities $\partial n_k/\partial\gamma_M$, the initial conditions depend on the curvature of the interface. If the interface at the point of incidence is plane, the third term on the right-hand side of (37*b*) vanishes. The quantities Y_{k3} and $\hat{Y}_{k3}$ contain first derivatives of elastic parameters, see (5). If the media, where incident and generated waves propagate, are homogeneous at the point of incidence, then Y_{k3} and $\hat{Y}_{k3}$ are zero. Note that (37*b*) must be applied even to unconverted transmitted waves across interfaces of the second order (across which elastic parameters vary continuously but their first derivatives; i.e, their gradients are discontinuous) since Y_{kM} change discontinuously across such interfaces. Through the quantities Y_{kM}, the initial conditions depend on the curvature of the incident wave front. For a plane incident wave front, Y_{kM} are zero. Through the terms $X_{k3}n_k$ the initial conditions depend on the angle of incidence of the incident wave. Note that the transformation equations cannot be used for grazing angles of either incident or generated waves since the terms $X_{k3}n_k$, and $\hat{X}_{k3}n_k$, respectively, which appear in denominators, become zero. If the variations of elastic parameters in the medium surrounding the interface are neglected (i.e., the interface is situated between homogeneous anisotropic media), equations (37) are equivalent to the formulae derived by *Norris* [1987]. Formulae (37) specified for an isotropic medium are equivalent to those derived by *Červený et al.*, [1974].

NUMERICAL EXAMPLES

In this section we present examples computed by solving the DRT equations. The DRT results are used here for several purposes. They are applied to evaluate the geometrical spreading, see (7) and (8), and to determine the coefficients of paraxial ray approximations (9) and (10). Moreover, DRT results are used in an interval ray-tracing procedure to determine the initial angles of rays connecting the source with points in specified intervals on a profile.

Computational Procedure

Program package SEISAN88 derived from program package SEISAN87, for details, see *Gajewski and Pšenčík* [1987, 1988], was used for the computations. Both packages are based on the ray method and allow computations of seismic body waves propagating in general 3-D laterally varying layered anisotropic structures.

Package SEISAN88 differs from SEISAN87 in the following aspects: The geometrical spreading and the coefficients of parax-

ial ray approximation are determined by numerical solution of the DRT equations (13) with (17), (18) (in SEISAN87, these quantities were evaluated approximately from nearby rays). A modified Euler method is used to integrate the DRT equations. The transformation of the DRT across interfaces is performed using (37).

Interval ray tracing is used to find the rays terminating along a prescribed profile. The procedure requires the termination of rays on a "termination surface", on which the profile is situated (e.g., for profiles on the free surface, the termination surface is the free surface). Rays are considered as terminating on the profile if their termination points are situated within a specified vicinity of the profile. The interval ray tracing procedure itself is based on formulae for two-point ray tracing of paraxial rays, see, e.g, *Červený et al.* [1984, 1988]. Similar formulae were recently used for two-point ray tracing for earthquake location in inhomogeneous isotropic media by *Virieux et al.* [1988]. In the interval ray tracing, an iterative loop is used, in which the initial slowness vector is changed at each step according to the above mentioned formulae, to find the ray arriving at the profile within an a priori specified vicinity of the termination point of the preceding ray. Unless the termination point is situated close to a caustic or a shadow zone of the considered wave, the procedure works reliably and fast. Travel times and vectorial amplitudes at an arbitrary receiver on the profile are then determined by paraxial ray approximation. The procedure is more effective for arrays of receivers rather than for single, scattered receivers.

In addition to the "surface profile" mode used in SEISAN87, the present program package allows also the calculation of synthetics along vertical profiles (the vertical seismic profiling (VSP) mode). In the VSP mode, the termination surface is a vertical cylinder with its axis passing through the source and with the radius equal to the offset of the source from the borehole.

For the surface profile mode as well as for the VSP mode the same wave code describing different elementary waves is used. The code corresponds to the one suggested by *Červený et al.* [1977]: Each segment of a ray is described by an integer, the absolute value of which specifies the layer number in which the segment is to be situated. Positive sign of the integer indicates a P or quasi P wave, negative sign specifies an S or any of the quasi S waves along the considered segment of the ray. In this way, for a given code, at any point of reflection/transmission in an anisotropic layer both quasi-shear waves are automatically generated. The interpretation of the wave code in the VSP mode is different from the surface profile mode. The intersection of a ray with the termination surface is accepted as a termination point of the ray only if the remaining part of the wave code (from the intersection with the termination surface to the surface of the model) does not contain any reflection or conversion instruction. This simple rule guarantees that termination points corresponding to different elementary waves (specified by different codes) cannot correspond to the same arrivals.

Let us add that for vertical seismic profiling the ray method for anisotropic media has already been applied by *Leary et al.* [1987] and *Li et al.* [1987]. They used it for the computation of P wave travel times and polarization vectors.

Model, Sources, Receivers, and Considered Waves

Let us consider a Cartesian coordinate system with the x and y axis horizontal and the z axis vertical, positive downward. The positive orientation of the x axis is to the east, of the y axis to the south, so that the system is right-handed. The model itself is situated in a cube. Its northwest upper corner corresponds to the origin of the Cartesian coordinate system. The length of an edge of the cube is 5 km. The top side of the cube represents the free surface, the bottom side the bottom of the model. Vertical sides of the cube form vertical boundaries of the model.

The model consists of four layers separated and/or limited by five interfaces. In Figure 1, a SW-NE vertical cross section of the model is shown. Interface 1 represents the free surface. Interface 2, forming the bottom of layer 1, is horizontal, situated at z=0.5 km depth. Interface 3 has a symmetric hill-shaped form with its top at x=2.5 km, y=2.5 km and at a depth of z=0.9 km.

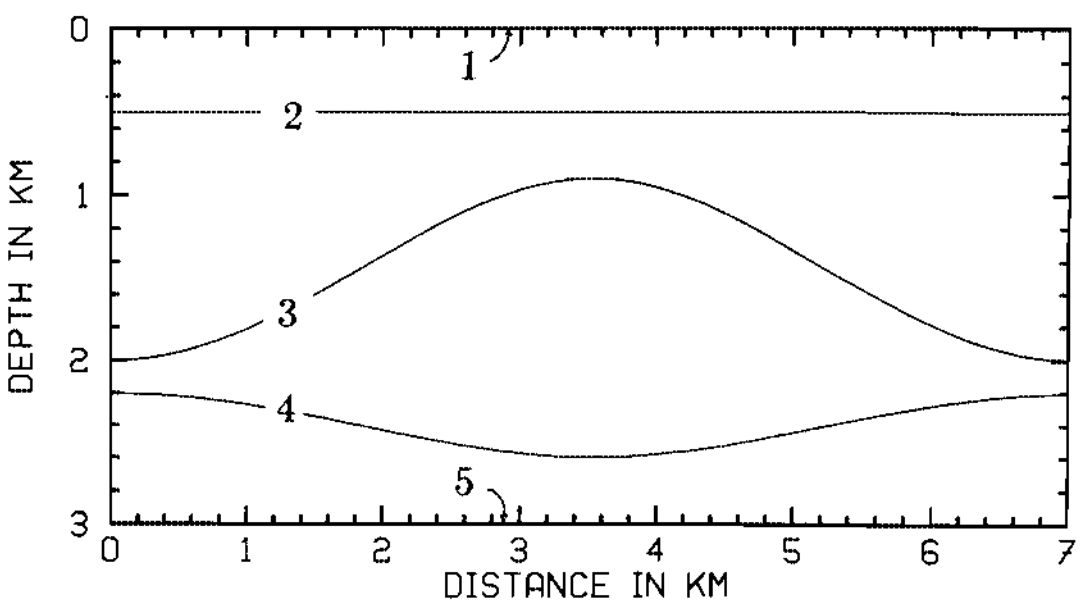

Fig. 1. SW-NE vertical cross section of the model through the symmetry axis of lateral heterogeneity. Numbered curves are interfaces.

Interface 3 intersects the vertical boundaries of the model along horizontal lines at a depth of 2.0 km. Interface 4 has a trough-shaped form with the deepest point at x=2.5, y=2.5 km and a depth of z=2.6 km. The interface intersects the vertical boundaries of the model along horizontal lines at a depth of z=2.2 km. Interface 5 coincides with the bottom of the model. With respect to the geometry of the interfaces, the model is thus axially symmetric with a vertical symmetry axis through x=2.5, y=2.5 km. Individual interfaces are specified by values of their depth at points on horizontal rectangular grids. Between these points, bicubic spline interpolation is used.

There is no lateral variation of elastic parameters inside layers. The elastic parameters are chosen such that the maximum vertical gradient of phase velocities does not exceed 0.04 s^{-1}.

The first layer is homogeneous, isotropic with P and S wave velocities equal to 3.8 and 2.0 km/s.

The second layer is formed by aligned water-filled cracks in an isotropic host rock. The crack density is 0.08 and the aspect ratio is 10^{-4}. The strike of the cracks is 140° (measured clockwise from the north) and the dip is 71°, with cracks dipping towards NE. The P-wave velocity of the host rock is 4.1 km/s at z=0.5 km, the constant vertical gradient is 0.03 s^{-1} and the v_p/v_s ratio is 1.783. Such a composition of layer 2 makes it effectively anisotropic, with hexagonal symmetry [*Hudson*, 1981; *Crampin*, 1984]. The axis of symmetry deviates from the horizontal plane by 19°. Resulting density–normalized elastic parameters were obtained from *Hudson's* [1981] formulae. The parameters are given in the coordinate system associated with the crystal axes (so that only five parameters are independent and the symmetry axis is considered as the x axis in the crystal coordinate system). The dimension of the density–normalized elastic parameters is given in $(km/s)^2$; compressed notation is used. At a depth of z=0.5 km we have A_{11}=16.80, A_{22}=16.81, A_{44}=5.29, A_{55}=4.42, and A_{12}=6.23; and at a depth of 6.5 km, we have A_{11}=18.48, A_{22}=18.49, A_{44}=5.81, A_{55}=4.85, and A_{12}=6.87. Between these depths the parameters are linearly interpolated.

Layer 3 is also anisotropic due to aligned water-filled cracks with a crack density of 0.05 and an aspect ratio of 10^{-4}, with the same orientation of the cracks as in layer 2. The P wave velocity of the host rock at z=3.5 km is 5.1 km/s, the vertical gradient of the P wave velocity is constant (0.03 s^{-1}) and the v_p/v_s ratio is 1.712. Resulting density–normalized elastic parameters at depth z=0.5 km are A_{11}=24.98, A_{22}=25.00, A_{44}=8.53, A_{55}=7.60, and A_{12}=7.94; and at depth z=6.5 km they are, A_{11}=27.02, A_{22}=27.04, A_{44}=9.24, A_{55}=8.24, and A_{12}=8.55 .

Layer 4 is homogeneous and isotropic with P wave velocity of 6.0 km/s and S wave velocity of 3.46 km/s.

To show the effects of anisotropy, synthetics computed for the above described model are compared with synthetics for a reference isotropic model. The velocity distribution of the reference model was obtained by averaging the phase velocities of the anisotropic model. In such a way, in layer 2 the P wave velocity at z=0.5 km is 4.1 km/s and the vertical gradient is 0.03 s^{-1}, S wave velocity is 2.2 km/s, and the vertical gradient is 0.016 s^{-1}. In layer 3, at z=3.5 km, these parameters in the same order are 5.1 km/s, 0.03 s^{-1}, 2.9 km/s, and 0.02 s^{-1}.

Single force point sources of unit strength are located at the free surface (the effects of the free surface at the source are not considered). Three different orientations of the single forces were used: vertical force pointing downward, radial force along the line connecting the source and the mouth of the borehole, pointing away from the source, and transverse force perpendicular to the previous two forces and orientated so that all three forces form a right-handed system. As a source time function, the Gaussian envelope signal [*Červený et al.*, 1977] with a prevailing frequency of 50 Hz and γ=4 is used. No phase or time shift is applied, so that the signal is cosine shaped and its arrival time corresponds to the maximum amplitude of the envelope of the signal.

Three-component receivers are located in the vertical borehole in the depth range from 0.15 to 2.55 km with 100-m spacing. Let us note that an arbitrarily curved borehole could be considered without any problem. The receivers are orientated as follows: the vertical component is positive upward, the radial component is orientated along the line connecting the source and the mouth of the borehole, positive away from the source, and the transverse component is orientated so that the system is right–handed.

All primary reflected unconverted waves including direct waves are considered. We consider as converted only those waves which at an interface transform from compressional (quasi-compressional) to shear (quasi-shear) or vice versa. The waves propagating only in isotropic layers are denoted by P or S, the waves propagating, at least partially, in anisotropic layers are denoted by qP, $qS2$ and $qS1$ ($qS2$ corresponds to the fastest quasi-shear wave, $qS1$ corresponds to the slowest quasi-shear wave). Let us recall that the wave code described above automatically includes both quasi-shear waves generated in each anisotropic layer. A subscript d indicates a direct wave. The integer subscript in the name of wave indicates the number of the interface where the wave was reflected. In this way, $qS2_3$ denotes the fastest quasi-shear wave reflected at the interface 3.

VSP Computations

The geometry of the VSP experiment is schematically shown in Figure 2. The borehole intersects the free surface at the point H with coordinates x=2.64 and y=2.77 km. S denotes the point of intersection of the vertical axis of symmetry of interfaces (and thus the axis of symmetry of lateral heterogeneity) with the free surface. Symbol $\vec{s}$ denotes the strike of aligned cracks, which makes 140°, and $\vec{d}$ denotes the projection of the dip vector of the cracks into the horizontal plane; the dip is 71° measured from the horizontal plane.

Two locations of point sources at the free surface are considered. Source A is situated at x=2.0 and y=2.0 km, source B at x=1.7 and y=2.42 km. In both cases, the offset of the source from the borehole is 1 km. For source A, the azimuth of the line connecting the source and the borehole is E50°S. This line is situated nearly in the plane of symmetry of lateral heterogeneity of the model and is perpendicular to the surface projection of the symmetry axis of the effectively anisotropic material in layers 2 and 3. Synthetics for this case will be thus more influenced by anisotropy than lateral heterogeneity. For source B, the line connecting the source and the borehole makes an azimuth of E20°S. Here the effect of lateral heterogeneity is expected to be greater.

Ray diagrams. Figures 3 and 4 show ray diagrams. Figure 3 corresponds to source A, Figure 4 to source B. There are two frames for each wave. The bottom frame shows projections of rays into the vertical plane containing the borehole and the source; interfaces are not plotted. The top frame shows projections of rays into the horizontal plane. The horizontal axis of the frame coincides with the line connecting the source and the

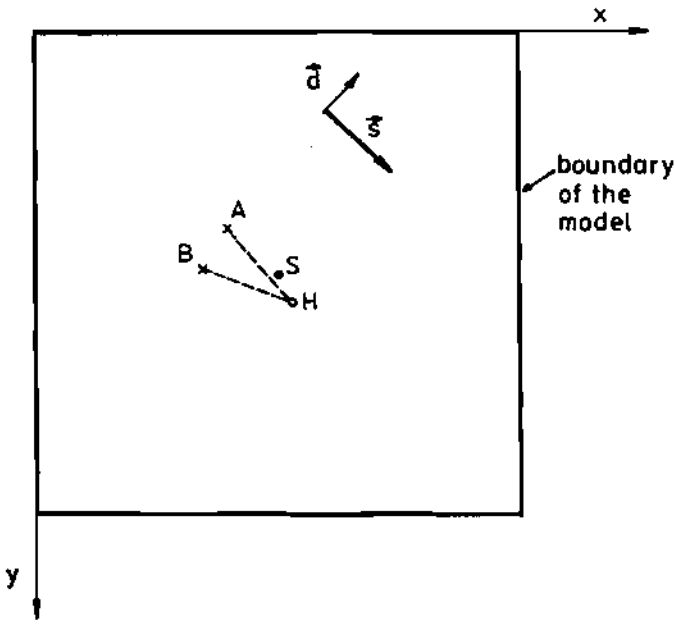

Fig. 2. Scheme of VSP experiment: H mouth of the borehole; A and B locations of single-force point sources; S intersection of the axis of symmetry of lateral heterogeneity with the free surface; $\vec{s}$ strike of the cracks (140°, measured clockwise from the north), $\vec{d}$ horizontal projection of the dip vector (dip of cracks is 71°, cracks are dipping towards NE).

borehole (s-b line in the following). In Figures 3*a*, 3*c*, 4*a*, and 4*c*, ray diagrams of the slowest direct quasi-shear wave ($qS\,1_d$) and the slowest quasi-shear wave reflected at the interface 4 ($qS\,1_4$) of the anisotropic model are shown. Figures 3*b*, 3*d*, 4*b*, and 4*d* show the ray diagrams of direct shear wave (S_d) and the shear wave reflected from interface 4 (S_4) propagating in the isotropic reference model.

The slowest direct quasi-shear wave generated by source A ($qS\,1_d$, see Figure 3*a*) is traveling in an isotropic homogeneous layer down to a depth of 0.5 km. The projections of its rays into the horizontal plane thus coincide with the s-b line. The projections into the vertical plane are straight lines. The rays, which penetrate below 0.5 km, propagate in an anisotropic medium, and therefore the projections of these rays into the horizontal plane deviate from the s-b line. The deviation attains almost 50 m. The projection of rays into the horizontal plane do not always terminate exactly on the borehole since acceptable rays can arrive in a prescribed finite vicinity of a profile.

The effects of anisotropy can be seen by comparison of Figures 3*a* and 3*b*. There are no great differences in projections of rays into the vertical plane. The projections of rays into the horizontal plane differ, however, substantially. The lateral variations of the isotropic reference model also produce deviations of rays from the s-b line, but for this configuration the deviations are much smaller than those of Figure 3*a*.

The same conclusion follows from the comparison of the ray diagrams for the $qS\,1_4$ and S_4 waves in Figures 3*c* and 3*d*. Note that here the deviations from the s-b line caused by anisotropy and lateral variations make almost 0.5 km on the horizontal distance of 1 km, whereas in the isotropic reference model the deviation caused by the lateral variations alone are about 50 m.

The effects of lateral heterogeneity are more pronounced, and at the same time the effects of anisotropy are weaker for rays shot from source B (see Figure 2). The same set of rays as in Figure 3 is shown in Figure 4, but for a source located at B. The ray diagrams for the anisotropic model and the isotropic reference model differ for this example much less than for the source located at A.

Time-distance curves. A set of time-distance curves of the considered waves from source A is shown in Figure 5*a*. Nearly parallel curves denoted by $qS\,1_d$, $qS\,2_d$, $qS\,1_3$, $qS\,2_3$, $qS\,1_4$, and $qS\,2_4$ are the time-distance curves of the slowest and fastest quasi-shear waves of the corresponding type. The time-distance curves of all other quasi-shear waves specified by the same wave code are situated between these curves. As evident from synthetics, some of these waves have negligible amplitudes. The time-distance curve of the direct quasi-shear wave splits below the 0.5 km level, where the wave enters anisotropic medium. The time difference between the slowest and fastest quasi-shear waves increases with the depth attaining almost 100 ms at a depth of 2.5 km.

In Figure 5*b*, a set of time-distance curves of the considered waves generated by source A in the reference isotropic model is shown. Compared with Figure 5*a*, the most prominent feature is the absence of splitted shear waves. It is interesting to note that although the ray paths in the anisotropic model deviate much more from the s-b line than the ray paths in the reference isotropic model (see, e.g., Figure 3*c* and 3*d*), the differences between corresponding time-distance curves are small (see, e.g., curve $qS\,1_4$ in Figure 5*a* and S_4 in Figure 5*b*). The same conclusion would follow from a similar comparison of wave fields generated by source B.

VSP synthetics. In Figures 6 and 7, three-component multisource VSP synthetics are shown. Each figure contains nine frames organized in three columns corresponding to the radial, transverse, and vertical single-force point sources. The frames in lines, from the top to the bottom, correspond to radial, transverse, and vertical components of the displacement vector. No amplitude power scaling is used; true amplitudes are presented. As the most energetic phases are the direct waves and the reflections from interfaces 2 and 3, a time range from 0.2 to 1.2 s was chosen (note that the time-distance curves in Figure 5 show times between 0 and 2 s).

In Figure 6*a*, VSP synthetics for source A located in the anisotropic model and in Figure 6*b* in the reference isotropic model are shown. The most prominent feature of "anisotropic" synthetics is the distribution of energy over all frames while in "isotropic" synthetics some frames are practically empty. This phenomenon is due to the nonvertical orientation of cracks. A similar observation in VSP data was made by *Majer et al.*, [1988] and was interpreted by *Shearer* [1988] also as a result of a nonvertical dip of aligned cracks.

The picture does not change much even for source B (Figure 7), although the lateral heterogeneity plays a more important role here.

The distribution of energy over all frames of three-component multisource synthetics is the best observable effect of anisotropy for the considered model and source locations. It is directly related to the orientation of the cracks.

In Figures 6*a* and 7*a*, shear wave splitting of the direct quasi-shear waves and the reflected quasi-shear waves from interface 3 can be also observed. A high-frequency signal (in our example the prevailing frequency was 50 Hz) is necessary to obtain splitted quasi-shear wave arrivals. For lower frequencies, the arriving quasi-shear waves would interfere which would complicate the detection of shear wave splitting.

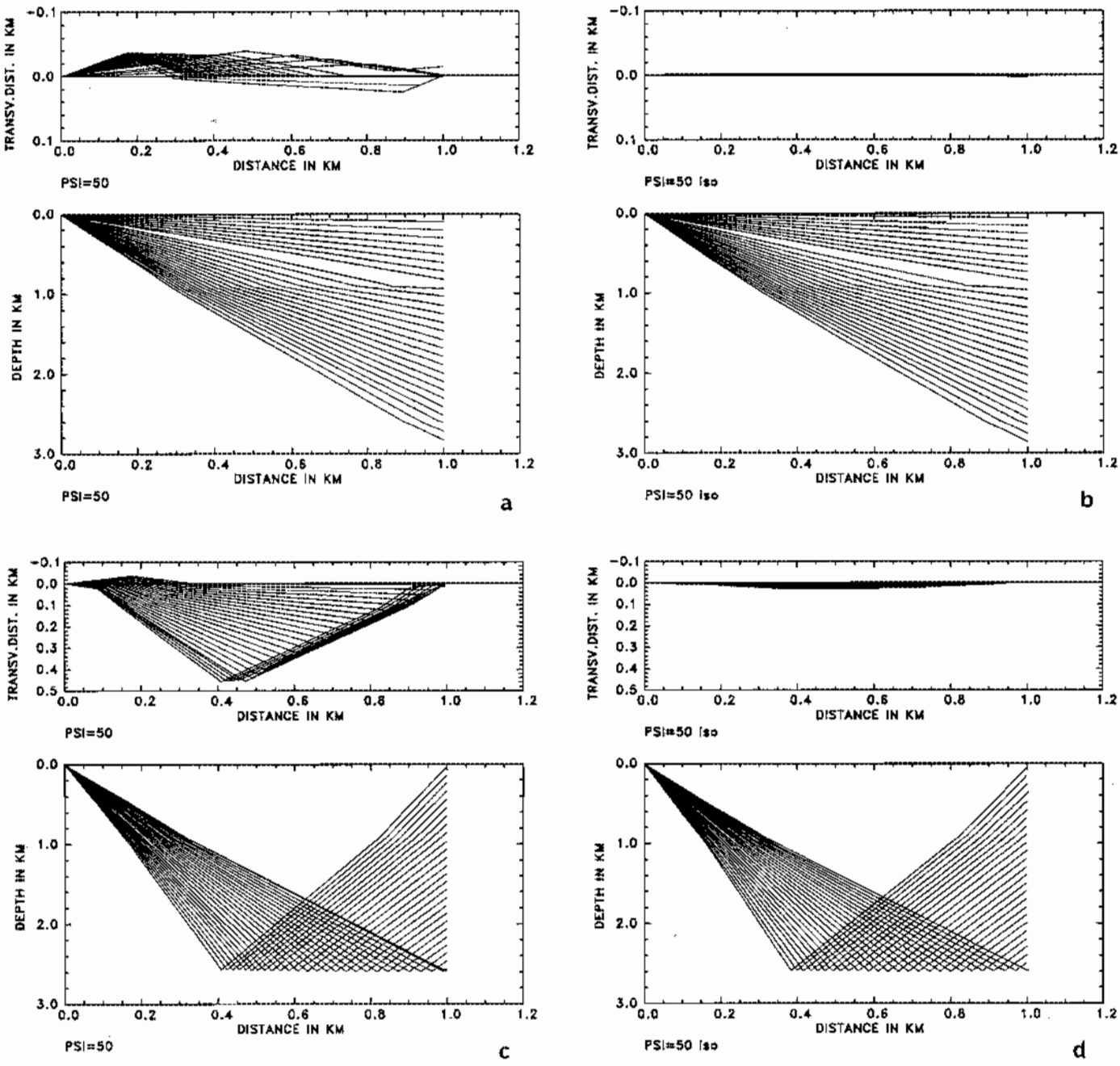

Fig. 3. (*a*) (*c*) Ray diagrams of quasi-shear waves in the anisotropic model and (*b*) (*d*) of shear waves in the reference isotropic model for source location A. Ray diagrams of (*a*) the slowest direct quasi-shear wave, (*b*) the direct S wave, (*c*) the slowest quasi-shear wave and (*d*) S wave reflected from the fourth interface. (Top) projections of rays into a horizontal plane; the horizontal axis corresponds to the line connecting source and borehole. (Bottom) projections of rays into the vertical plane containing the borehole and the source.

DISCUSSION

The ray method is an effective tool to compute seismic wave fields propagating in anisotropic media. Memory requirements of ray codes are minimum (program package SEISAN88 needs a few hundred kilobytes of core memory) so that they can be used even on personal computers. The ray computations are fast, in comparison with the reflectivity method or finite difference methods faster by a few orders (CPU time for synthetics presented in the previous section using a nonvectorized package SEISAN88 on a CONVEX C1 computer was about 200 s). The ray computations can be performed for models of sufficiently realistic structures and realistic extent. The ray computations give a clear insight into the formation of the wave field and allow an easy identification of individual phases forming the wave field. It is not difficult to incorporate effects of slight absorption into the ray computations.

When considering the ray synthetics presented in the previous section, one must be, however, aware of the following facts. It is well known that the ray method is only approximate and it does not work properly or it even fails in singular regions (critical regions, caustic regions, transitions from the illuminated to

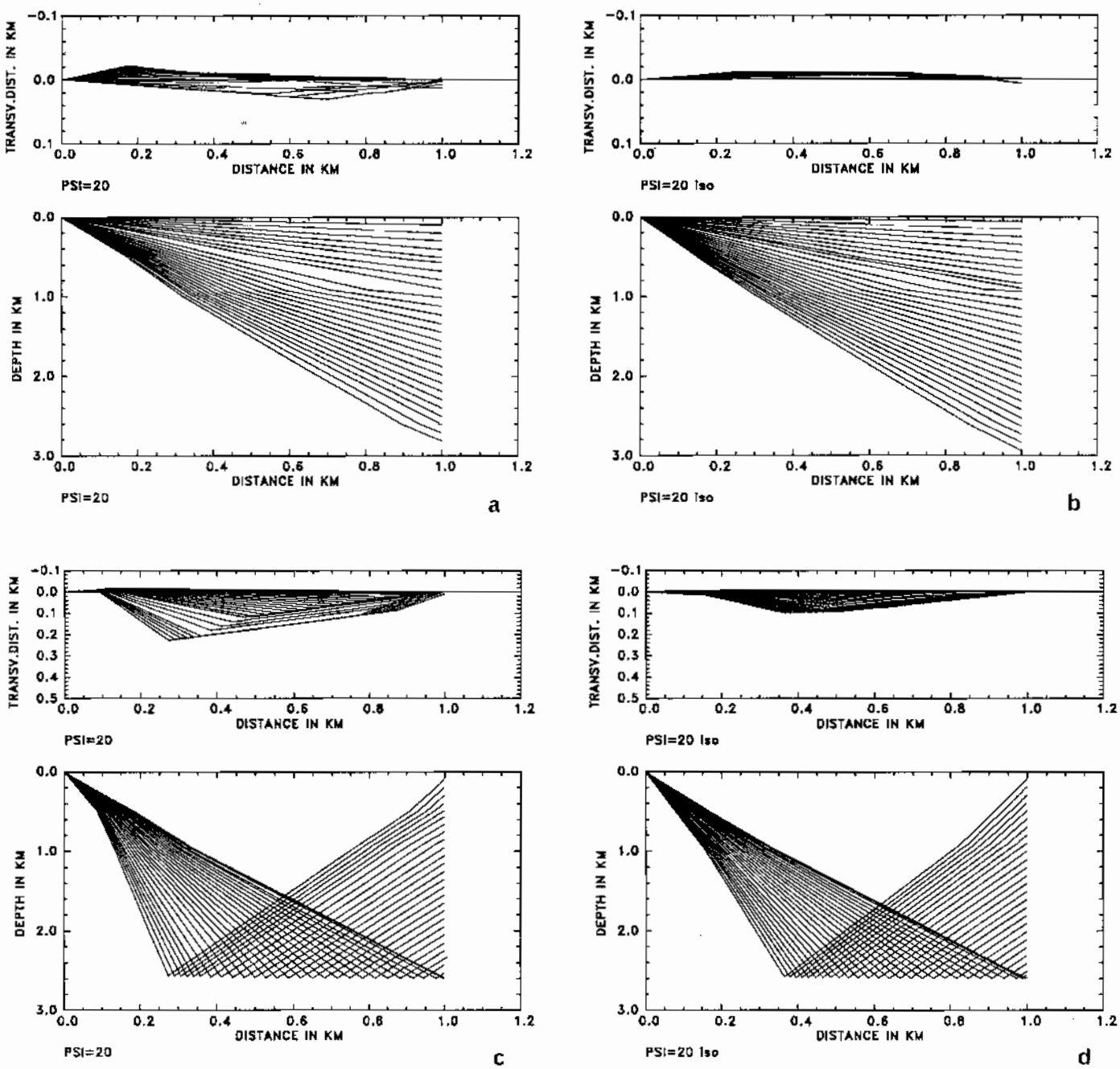

Fig. 4. The same as in Figure 3, but for source B.

shadow regions). In inhomogeneous anisotropic media, the ray method does not work properly for quasi-shear waves in regions or directions, in which both these waves propagate with nearly the same phase speed and are, therefore, coupled [*Kravtsov and Orlov*, 1980; *Chapman and Shearer*, 1989]. The problems connected with singular regions may be overcome by the application of some modifications or generalizations of the ray method such as the Gaussian beam summation method or Maslov method. The problem of coupled quasi-shear waves is more complex and will require a special treatment. For example, for weakly anisotropic media, *Kravtsov and Orlov* [1980] suggest a modification called quasi-anisotropic ray approximation which is closely related to the perturbation theory.

In this paper the standard ray method was used. Even without any modification, its results may be of significant value if parts of the seismic wave field distorted by singularities can be identified. The identification of effects of singular regions which commonly occur in isotropic media is not difficult. For the identification of regions of quasi-shear wave coupling, we used a rough rule, modified from *Kravtsov and Orlov* [1980], where it was suggested for harmonic waves. Quasi-harmonic waves can be considered uncoupled if the following condition is satisfied

$$f^{-1} V \left| \nabla V \right| \ll \left| \Delta V \right|$$

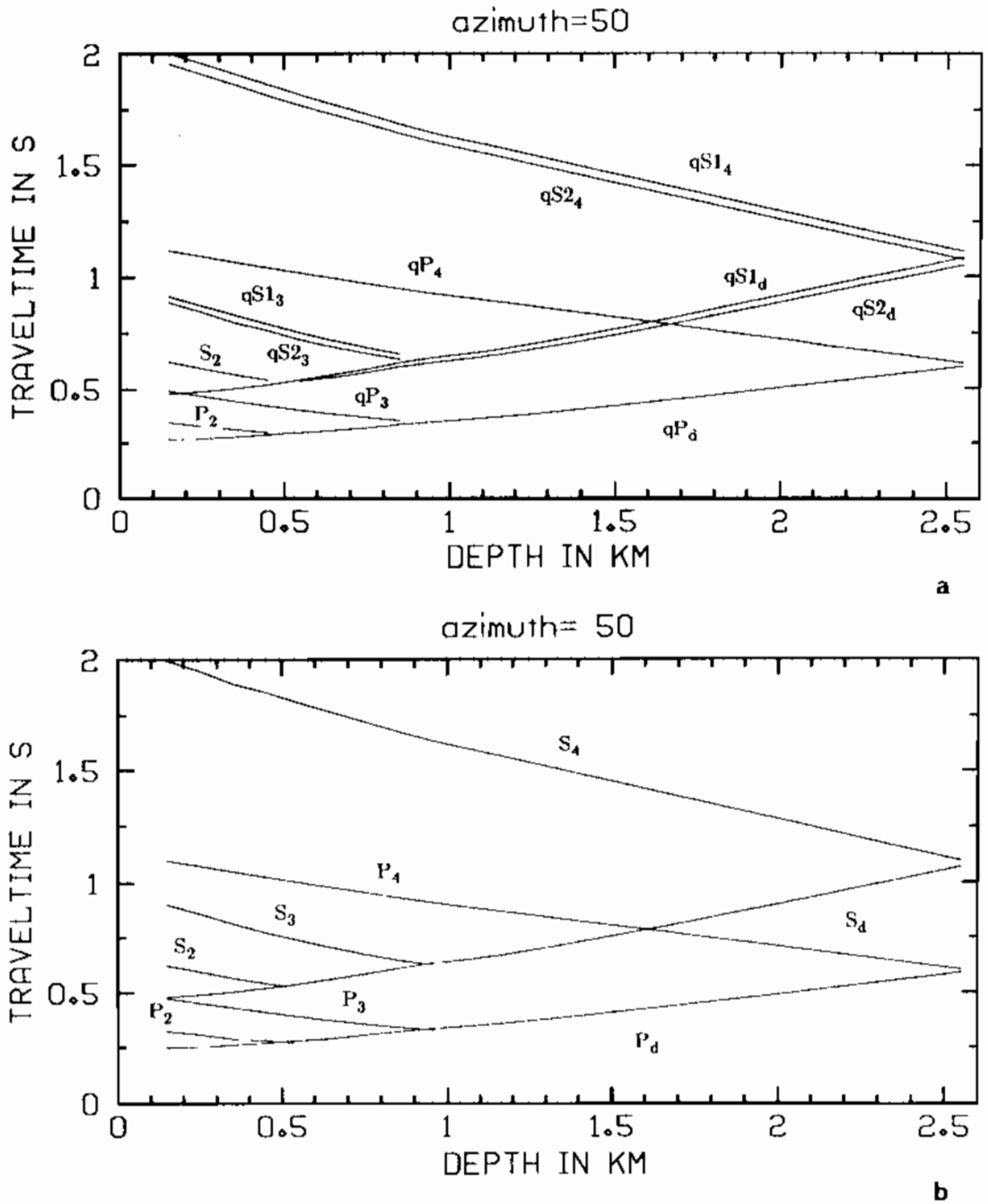

Fig. 5. Time-distance curves of waves generated by the source located at A (*a*) in the anisotropic model and (*b*) in the reference isotropic model. For details see text.

Here V denotes an average of phase velocities of both quasi-shear waves propagating in the same direction, ΔV is the difference between these phase velocities, and f is the prevailing frequency of the waves. The above inequality follows from the requirement that the distance on which the two quasi-shear waves separate by a prevailing wavelength be considerably smaller than the distance on which the phase velocities change by an amount equal to V.

The above criterion can be easily tested in each step of the ray tracing procedure. For practical use, it is necessary to specify the meaning of "considerably less". In our computations we considered the inequality satisfied if its left-hand side was at least 10 times less than its right-hand side. For illustration, in Figure 8 we show a distribution of quasi-shear wave phase velocities in dependence on the angle of incidence of a downgoing wave with the angle measured from the horizontal. The phase velocities are calculated for a depth of 2.0 km. Different symbols correspond to different profiles. We can see that for the profile from source A (azimuth E50°S), the difference of both phase velocities is not less than 0.1 km/s. In this case the left-hand side of the above inequality is 0.0013 (average phase velocity is about 2.2 km/s, gradient is 0.03 s^{-1}, and prevailing frequency is 50 Hz), i.e., about 75 times less than the smallest difference in phase velocities. For the profile from source B (azimuth E20°S), the difference in phase velocities is minimum for a horizontal path and amounts to 0.02 km/s.

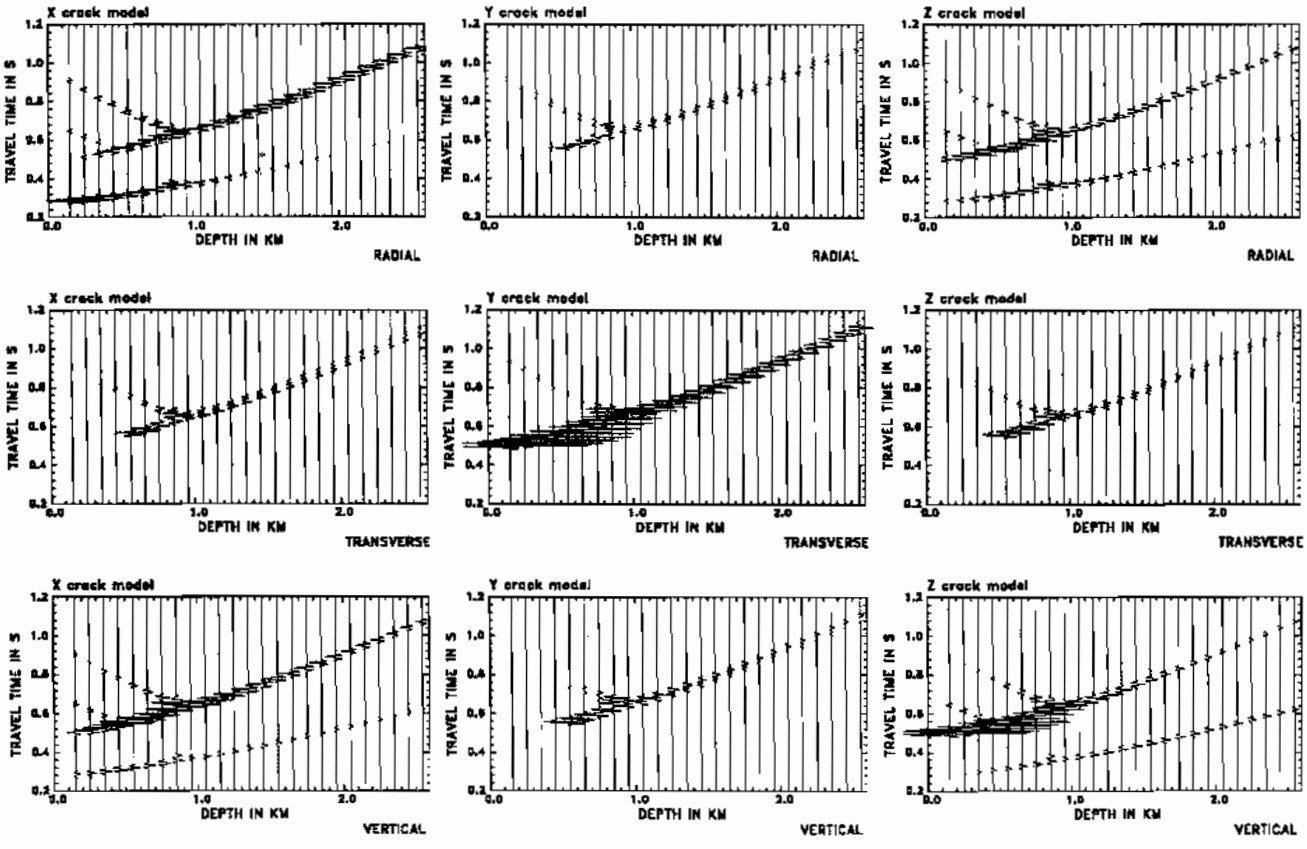

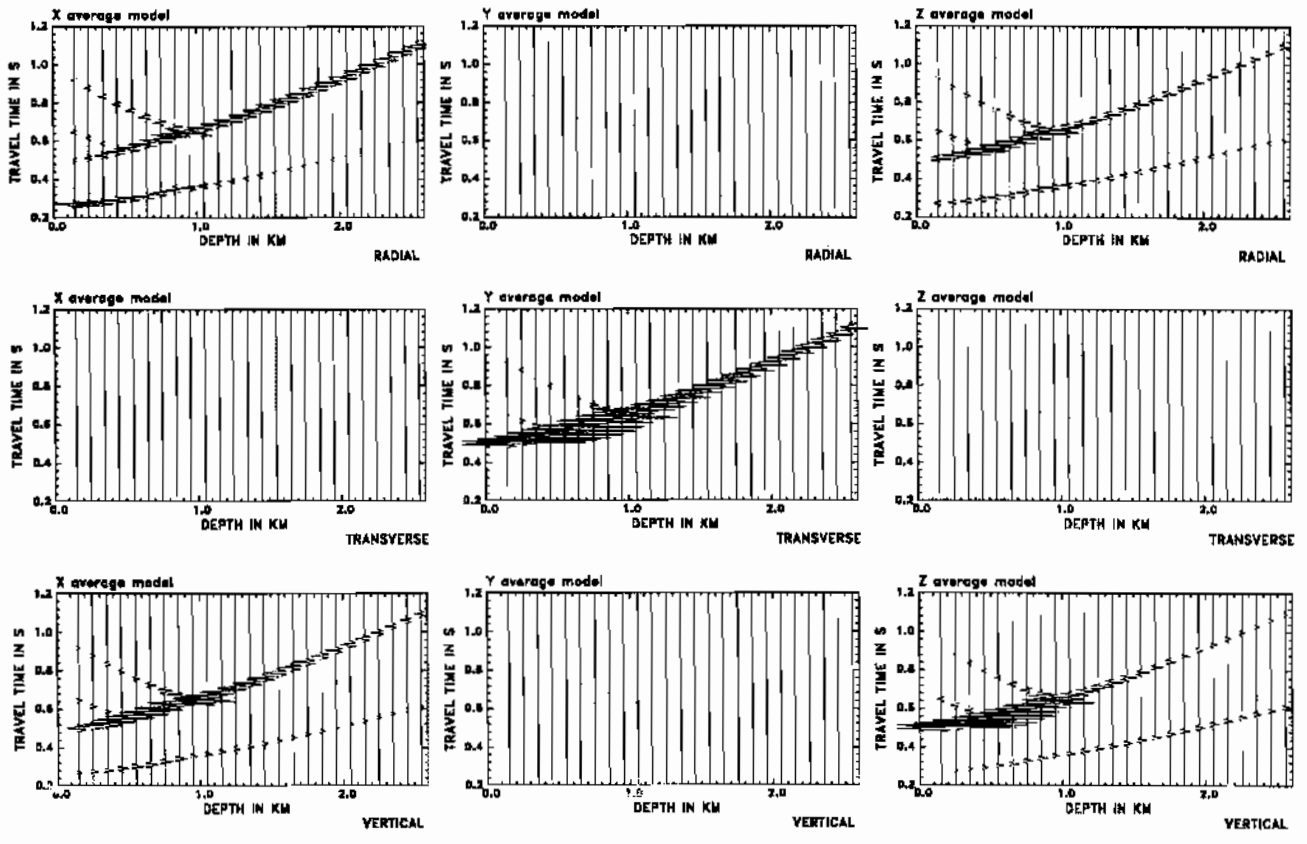

Fig. 6. Multisource three-component VSP synthetics generated by source A (*a*) in the anisotropic model and (*b*) in the reference isotropic model. Columns from left to right correspond to radial, transverse, and vertical single-force sources; the lines from top to bottom correspond to radial, transverse, and vertical components of the displacement vector.

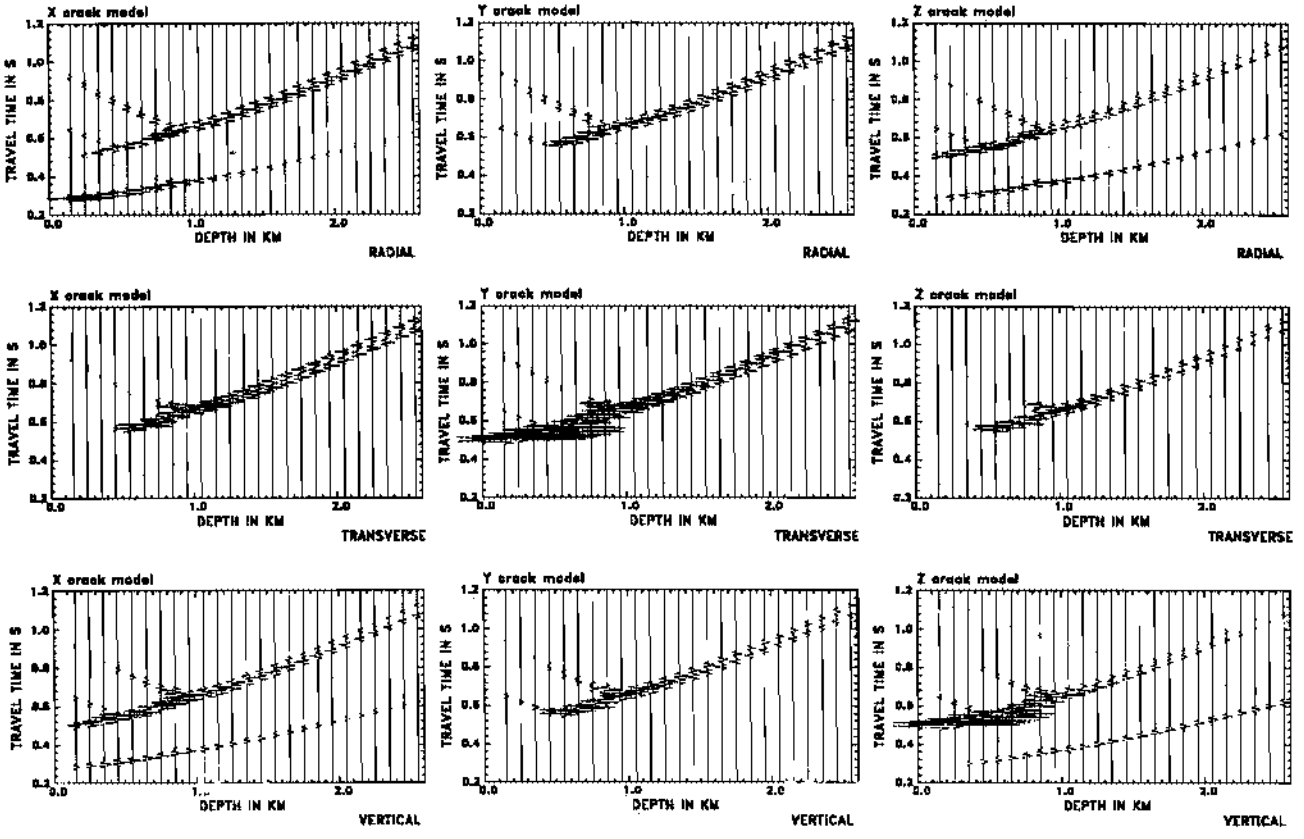

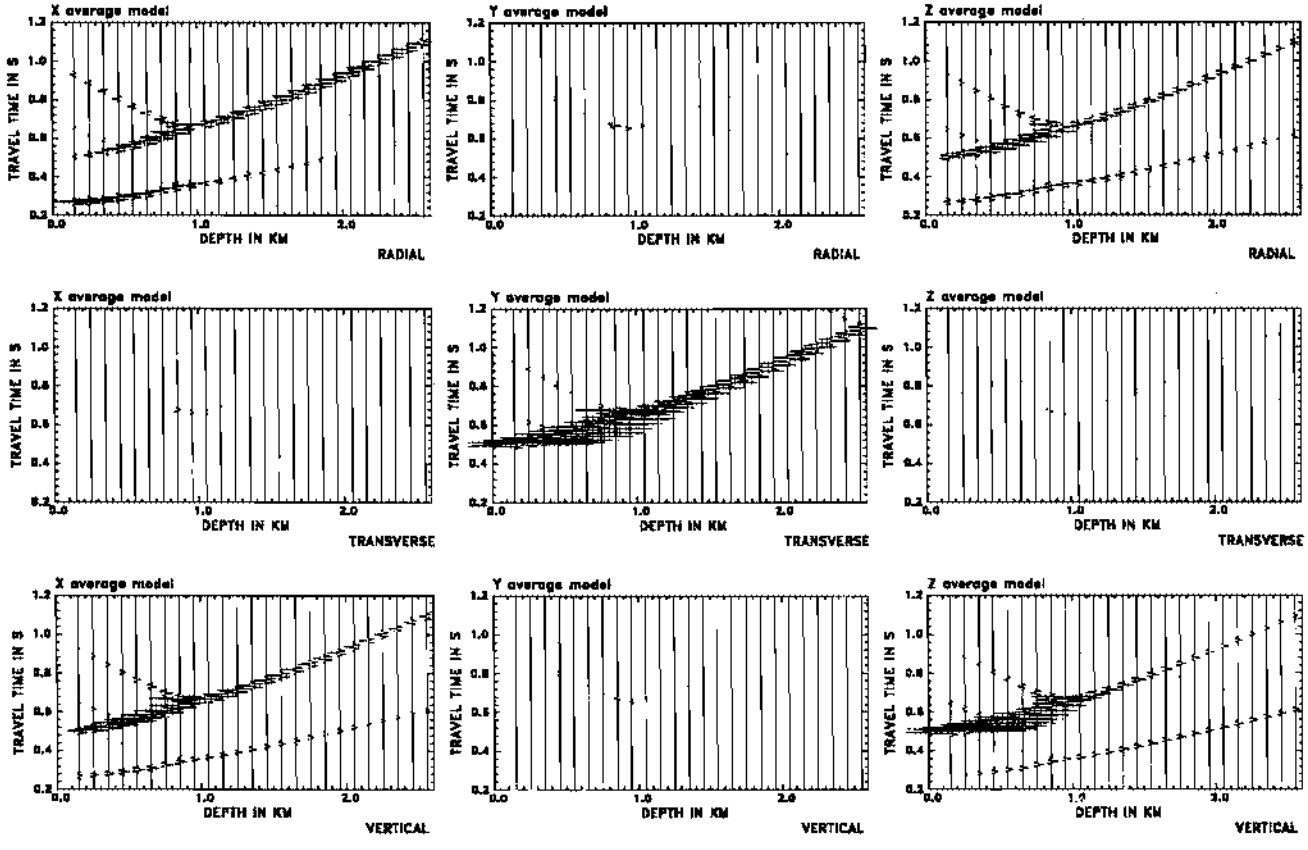

Fig. 7. The same as in Figure 6, but for source B.

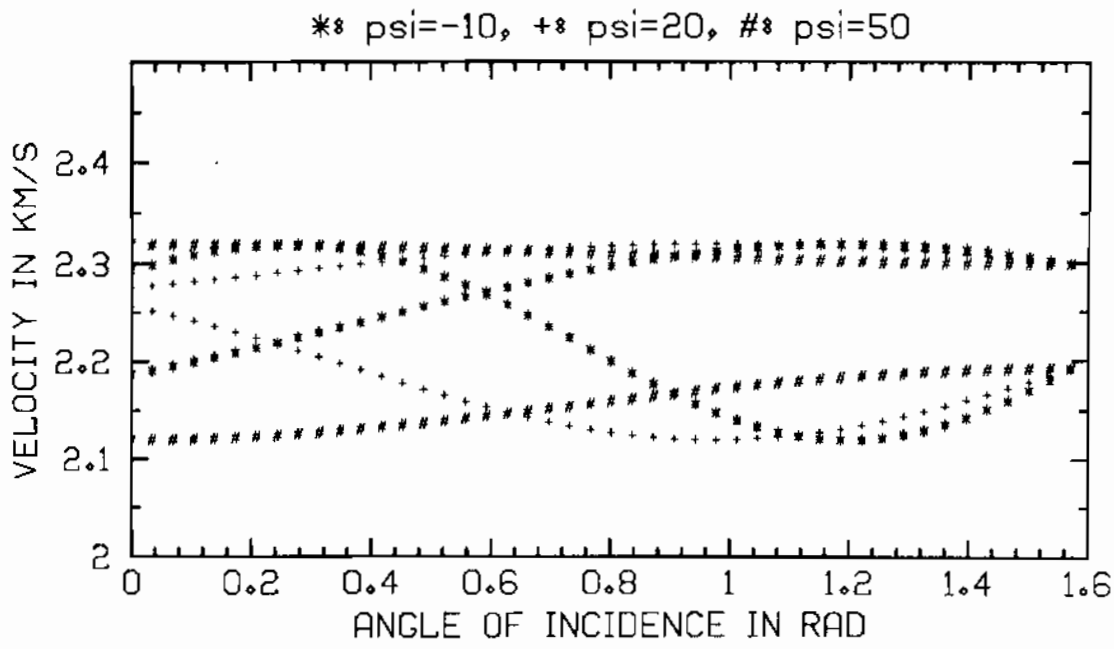

Fig. 8. Distribution of phase velocities of the two quasi-shear waves propagating along downgoing rays in the second layer of the anisotropic model at a depth of 2 km. Independent variable is the angle of incidence, measured from the horizontal. Number signs correspond to source A, crosses correspond to source B, and asterisks correspond to the source situated on the profile through the borehole with an azimuth of N80°E.

In this case the right-hand side is about 15 times greater than the left-hand side. Computations for the profile with an azimuth of N80°E (not presented here) contain distortions due to the coupling of quasi-shear waves for the angles close to 0.6 rad. Even in this case, travel times are not affected.

All the above estimates require, of course, further investigations, both by comparing the ray results with the results of more exact methods and by direct analysis of ray formulae describing the behavior of quasi-shear waves in regions of coupling, see *Chapman and Shearer* [1989].

Another phenomenon which may affect the computed wave field is the effect of the free surface at the source. As mentioned above, in this study we neglected this effect. We intend to incorporate it and study its influence in a forthcoming paper. For any *P* wave and for *S* waves inside the source shear wave window, i.e., for shear waves leaving the source under an angle less than the angle of critical *SP* reflection from the free surface, the distortion is expected to be relatively small. Outside the window, the shear waves will be elliptically polarized. The probability for a receiver to be situated within such a window increases with increasing depth of the receiver and decreasing offset of the source from the borehole.

Finally, let us briefly explain why we use the wave code, which automatically includes both generated quasi-shear waves at each point of reflection or transmission in an anisotropic layer. In the algorithm used, the quasi-shear waves are identified by their phase speed. As can be seen from Figure 8, this identification may lead to a transfer from one phase sheet to the other even within a layer (see the intersection of phase velocity curves marked by asterisks). At a point of reflection or transmission, such a transfer is even more probable. In this way, if not all possible quasi-shear wave ray paths are considered, the resulting wave field is not complete and is distorted because all quasi-shear waves described by one code propagate close to each other and interfere (in Figure 5*a* all these waves interfere in the belt described by the fastest and slowest quasi-shear waves). We can close this section with the conclusion that in smooth anisotropic media, two splitted quasi-shear waves with different polarizations can be observed, whereas in general layered anisotropic media, quasi-shear waves are expected to form interference groups of variable polarizations.

APPENDIX

Let us consider the slowness vector of one of the three waves which may propagate in an anisotropic medium. The slowness vector is specified by the direction of a unit wave normal N_i and the phase velocity V of the considered wave in the specified direction so that $p_i=N_i/V$. Having p_i, we can calculate the matrix Γ_{jk}; see equation (4). The three eigenvalues $G^{(m)}$ of the matrix Γ_{jk} and their corresponding eigenvectors $g_j^{(m)}$ can be determined from the Christoffel equation

$$(\Gamma_{jk}-G^{(m)}\delta_{jk})g_k^{(m)}=0 \tag{A1}$$

Multiplying (A1) by $g_j^{(m)}$ and taking into account that the eigenvector $g_j^{(m)}$ is a unit vector, we get an explicit expression for $G^{(m)}$,

$$G^{(m)}=\Gamma_{jk}g_j^{(m)}g_k^{(m)}=a_{ijkl}p_ip_lg_j^{(m)}g_k^{(m)} \tag{A2}$$

From comparison of (A1) and (2), we can see that the slowness vector p_i of the considered mth wave and specifically its phase velocity V_m cannot be chosen arbitrarily. They must be chosen such that $G^{(m)}=1$; i.e., they must satisfy the eikonal equation (6). In this way, the equation (6) can be interpreted as an equation of the slowness surface of the considered wave. Using $p_i=N_i/V_m$, the eikonal equation can be rewritten in an alternative form,

$$a_{ijkl}N_iN_lg_j^{(m)}g_k^{(m)}=V_m^2$$

It follows from this equation that the three eigenvalues $G^{(j)}$ are given by the relation,

$$G^{(j)}=\left[\frac{V_j}{V_m}\right]^2$$

The eigenvalue corresponding to the considered wave ($j=m$) yields $G^{(m)}=1$ and thus justifies the eikonal equation (6). The other eigenvalues are generally different from unit. An exception is the case in which two quasi-shear wave slowness surfaces touch or intersect each other. Then their phase velocities are identical, $V_j=V_m$ for $j\neq m$, and the above equation yields $G^{(j)}=G^{(m)}=1$. On the contrary, equality of two eigenvalues implies equality of the corresponding phase velocities.

Let us now derive an expression for the second derivative of the eigenfunctions $G^{(m)}$, see (20), in terms of the complete system of eigenvalues $G^{(j)}$ and eigenvectors $g_k^{(j)}$. Differentiating equation (A1) with respect to z_s, where z_s may be either x_s or p_s, we get

$$\frac{\partial\Gamma_{jk}}{\partial z_s}g_k^{(m)}+\Gamma_{jk}\frac{\partial g_k^{(m)}}{\partial z_s}-\frac{\partial G^{(m)}}{\partial z_s}g_j^{(m)}-G^{(m)}\frac{\partial g_j^{(m)}}{\partial z_s}=0 \quad \text{(A3)}$$

If we multiply (A3) by $g_j^{(m)}$ and take into account (A1), we arrive at

$$\frac{\partial G^{(m)}}{\partial z_s}=\frac{\partial\Gamma_{jk}}{\partial z_s}g_j^{(m)}g_k^{(m)} \quad \text{(A4)}$$

which has already been used on the right-hand side of the ray–tracing equations (5). Comparing (A4) with the derivative of (A2), we get an identity

$$\Gamma_{jk}\frac{\partial g_j^{(m)}}{\partial z_s}g_k^{(m)}=0$$

Differentiating (A4) with respect to z_r, we get an expression for the second derivatives of $G^{(m)}$,

$$\frac{\partial^2 G^{(m)}}{\partial z_s\partial z_r}=\frac{\partial^2\Gamma_{jk}}{\partial z_s\partial z_r}g_j^{(m)}g_k^{(m)}+2\frac{\partial\Gamma_{jk}}{\partial z_s}\frac{\partial g_j^{(m)}}{\partial z_r}g_k^{(m)} \quad \text{(A5)}$$

This formula is useful as soon as we can determine $\partial g_j^{(m)}/\partial z_r$.

From the definition of eigenvector $g_j^{(m)}$ as a unit vector it simply follows

$$\frac{\partial g_j^{(m)}}{\partial z_s}g_j^{(m)}=0 \quad \text{(A6)}$$

It follows from (A6) that

$$\frac{\partial g_j^{(m)}}{\partial z_s}=\sum_{n=1}^{3}c_{mn}g_j^{(n)} \quad \text{(A7)}$$

where

$$c_{mn}=g_k^{(n)}\frac{\partial g_k^{(m)}}{\partial z_s} \quad \text{for } n\neq m$$
$$c_{mn}=0 \quad \text{for } n=m \quad \text{(A8)}$$

If we multiply (A3) by $g_j^{(n)}$ with $n\neq m$, take into account (A1) and assume $G^{(n)}\neq G^{(m)}$, we get for c_{mn},

$$c_{mn}=(G^{(m)}-G^{(n)})^{-1}\frac{\partial\Gamma_{jk}}{\partial z_s}g_k^{(m)}g_j^{(n)} \quad \text{(A9)}$$

Inserting (A9) into (A7), and the resulting relation into (A5), we arrive at the final expression for the second derivative of $G^{(m)}$,

$$\frac{\partial^2 G}{\partial z_r\partial z_s}=\frac{\partial^2\Gamma_{jk}}{\partial z_r\partial z_s}g_j^{(m)}g_k^{(m)}+2\sum_{n=1}^{3}{}^{(n\neq m)}(G^{(m)}-G^{(n)})^{-1}A_r^{(mn)}A_s^{(mn)} \quad \text{(A10)}$$

In (A10),

$$A_r^{(mn)}=\frac{\partial\Gamma_{jk}}{\partial z_r}g_j^{(m)}g_k^{(n)} \quad \text{(A11)}$$

which implies, see (A4),

$$\frac{\partial G^{(m)}}{\partial z_s}=A_s^{(mm)} \quad \text{(A12)}$$

The symbol $\sum_n^{(n\neq m)}$ in (A10) denotes the summation in which the term for $n=m$ is not included.

Acknowledgments. We are grateful to G.A. Thompson for the possibility to carry out this study at the Geophysics Department, Stanford University, and to J.F. Claerbout for permission to use the Stanford Exploration Project CONVEX computer. We thank V. Červený, J. Jech and L. Klimeš for critical reading of the manuscript and an anonymous reviewer for his comments. D. G. was supported by a grant from the German Research Society (DFG grant III 02-GA 350/1-1). This work was partially supported through U.S. Department of Energy Contract No. DE-AC03-76F00098 by the DOE Office of Civilian Radioactive Waste Management, Office of Geologic Repositories.

REFERENCES

Červený, V., Seismic rays and ray intensities in inhomogeneous anisotropic media, *Geophys. J. R. Astron. Soc., 29*, 1-13, 1972.

Červený, V., J. Langer, and I. Pšenčík, Computation of geometric spreading of seismic body waves in laterally inhomogeneous media with curved interfaces, *Geophys. J. R. Astron. Soc., 38*, 9-19, 1974.

Červený, V., I.A. Molotkov, and I. Pšenčík, *Ray Method in Seismology*, Charles University Press, Prague, 1977.

Červený, V., L. Klimeš, and I. Pšenčík, Paraxial ray approximation in the computation of seismic wavefields in inhomogeneous media, *Geophys. J. R. Astron. Soc., 79*, 89-104, 1984.

Červený, V., L. Klimeš, and I. Pšenčík, Complete seismic ray tracing in 3-D laterally layered structures, in *Seismological Algorithms*, edited by D.J. Doornbos, pp. 89-168, Academic, San Diego, Calif., 1988.

Chapman, C.H., and P.M. Shearer, Ray tracing in azimuthally anisotropic media, II, Quasi-shear wave coupling, *Geophys. J., 96*, 65-83, 1989.

Crampin, S., Effective elastic constants for wave propagation through cracked solids, *Geophys. J. R. Astron. Soc., 76*, 17-28, 1984.

Fedorov, F.I., *Theory of Elastic Waves in Crystals*, Plenum, New York, 1968.

Gajewski, D., and I. Pšenčík, Computation of high-frequency seismic wavefields in 3-D laterally inhomogeneous anisotropic media, *Geophys. J. R. Astron. Soc., 91*, 383-411, 1987.

Gajewski, D., and I. Pšenčík, Ray synthetic seismograms for a 3-D anisotropic lithospheric structure, *Phys. Earth Planet. Inter., 51*, 1–23, 1988.

Hanyga, A., Dynamic ray tracing in an anisotropic medium, *Tectonophysics, 90*, 243-251, 1982.

Hudson, J.A., Wave speeds and attenuation of elastic waves in material containing cracks, *Geophys. J. R. Astron. Soc., 64*, 133-150, 1981.

Kendall, J.-M., and C.J. Thomson, A comment on the form of the geometrical spreading equations, with some numerical examples of seismic ray tracing in inhomogeneous anisotropic media, *Geophys. J. Int.*, in press, 1989.

Kravtsov, Yu.A., and Yu.I. Orlov, *Geometrical Optics of Inhomogeneous Media* (in Russian), Nauka, Moscow, 1980.

Leary, P.C., Y.-G. Li, and K. Aki, Observation and modelling of fault zone fracture seismic anisotropy, I, *P*, *SV* and *SH* travel times, *Geophys. J. R. Astron. Soc., 91*, 461-484, 1987.

Li, Y.-G., P.C. Leary, and K. Aki, Observation and modelling of fault zone fracture seismic anisotropy, II, *P*-wave polarization anomalies, *Geophys. J. R. Astron. Soc., 91*, 485-492, 1987.

Majer, E.L., T.V. McEvilly, F.S. Eastwood, and L.R. Myer, Fracture detection using *P*- and *S*-wave VSPs at the Geysers geothermal field, *Geophysics, 53*, 76-84, 1988.

Nomofilov, V.E., Asymptotic solutions of the second order systems of differential equations concentrated in a vicinity of a ray (in Russian), in, *Mathematical Problems of Theory of Wave Propagation*, Vol. 11, pp. 170-179, Nauka, Leningrad, 1981.

Norris, A.N., A theory of pulse propagation in anisotropic elastic solids, *Wave Motion, 9*, 509-532, 1987.

Shearer, P.M., Synthetic seismogram modeling of shear-wave splitting in VSP data from The Geysers, California, *Geophys. Res. Lett., 15*, 1085-1088, 1988.

Virieux, J., V. Farra, and R. Madariaga, Ray tracing for earthquake location in laterally heterogeneous media, *J. Geophys. Res., 93*, 6585–6599, 1988.

D. Gajewski, Institute of Geophysics, Technical University of Clausthal, P.O. Box 1253, 3392 Clausthal-Zellerfeld, Federal Republic of Germany.

I. Pšenčík, Geophysical Institute, Czechoslovak Academy of Sciences, Boční II, 14131 Praha 4, Czechoslovakia.

(Received February 3, 1989:
revised July 26, 1989;
accepted April 10, 1989.)